ACS OMEGA

http://pubs.acs.org/journal/acsodf

Article

Conversion of a Helical Surface Plasmon Polariton into a Spiral Surface Plasmon Polariton at the Outlet of a Metallic Nanohole

Yun-Cheng Ku, Jiunn-Woei Liaw,* Szu-Yao Mao, and Mao-Kuen Kuo*

Cite This: *ACS Omega* 2022, 7, 10420−10428

Read Online

ACCESS | Metrics & More | Article Recommendations | Supporting Information

ABSTRACT: The conversion of a helical surface plasmon polariton (SPP) creeping out of a circular nanohole in a thick metal (Ag or Au) film into a spiral (Hankel type) SPP outward propagating at the film's interface is studied theoretically. The dispersion relations of SPPs of various modes in a nanohole, calculated from a transcendental equation, show that the propagation length of an SPP of mode 1 is much larger than the other modes in a specific frequency band, which is dependent on the nanohole size. In this band, the streamlines of the Poynting vector (energy flux) of mode-1 SPP in nanohole exhibit helixes; the surface component of the energy flux is perpendicular to the phase front of the SPP. Numerical results show that, after a helical SPP tunnels through a nanohole, most of the energy flux fans out at the outlet as a dipole radiation. The spatial phase distribution of E_z above the interface indicates that the transmission light carries orbital angular momentum with a topological charge of 1. Additionally, a part of the helical SPP creeping along the edge of an outlet naturally converts into a spiral (Hankel type of order 1) SPP outward propagating at the film's interface; both SPPs have the same handedness. Moreover, the interferences of multi SPPs generating from two nanoholes and even from a two-dimensional nanohole array are also related to the spiral SPP.

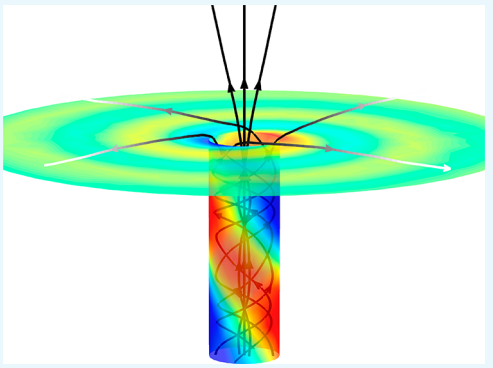

INTRODUCTION

The size-dependent color filter of a two-dimensional (2D) nanohole array in a metal film for light transmission was discovered by Ebbesen's experiments.[1−4] In the past decades, the related issues have been extensively studied.[5−13] The phenomena are found to be related to a surface plasmon polariton (SPP) propagating along nanoholes in a metal film.[14−16] On the one hand, Shin et al. found that the HE_{11} mode is the dominant propagating mode in a nanohole of a thick Ag film.[16] On the other hand, the SPP at the interface of a metal film induced by a transmission light via a metallic nanohole has been studied.[17−19] For example, Yin et al. used near-field scanning optical microscopy (NSOM) to measure an SPP originating from a nanohole at the upper interface of Au film irradiated by a linearly polarized (LP) light at the lower side.[17] In addition, Chang et al. used the finite-difference time-domain (FDTD) method to verify that this induced SPP can be approximated by a Hankel-type SPP of order 1 propagating at the upper interface of a thin Au film.[18] Häfele et al. used leakage radiation microscopy to measure the interference of SPPs from a pair of nanoholes; this result can be explained by the interference of two Hankel-type SPPs of order 1 originating from two nanoholes.[20,21] Furthermore, on the one hand, the interference of multi SPPs generated from the transmission light through a one-dimensional (1D) or 2D array of nanoholes in a Au film measured by NSOM has been reported.[22−24] On the other hand, the scattering light from two nanoholes and a 1D array of nanoholes in Au film were measured by dark-field microscopy.[25]

Several studies also reported that a Hankel-type SPP of order 1 can also be induced around a nanohole at the illumination side of a metal−dielectric interface, which is the scattering result of an incident light encountering a nanohole.[26,27] Recently, a circularly polarized (CP) plane wave in the terahertz regime carrying only spin angular momentum (SAM) via a subwavelength (square or circular) aperture in Al foil can produce a transmission in the near field carrying orbital angular momentum (OAM) through the spin−orbit interaction (SOI) of an electromagnetic field.[28] The phenomenon of SOI is indicated by the phase singularity of a longitudinal electric field. Wei et al. utilized a Laguerre−Gaussian (LG) light beam carrying OAM at λ = 633 nm to irradiate a single nanohole in a Au film and then detected the OAM of the transmission light on the backside of film at a long distance, for example, 120 μm.[29] These studies demonstrate that a metallic nanohole can facilitate the SOI of light to produce a transmission field with OAM at the near field or far field no matter whether the incident field carries OAM or not.[28−30]

Received: December 21, 2021
Accepted: March 3, 2022
Published: March 15, 2022

https://doi.org/10.1021/acsomega.1c07187
ACS Omega 2022, 7, 10420−10428

In this paper, we demonstrate that, via a sub-wavelength nanohole in metallic film, a light source without carrying OAM in the UV−vis−NIR (NIR = near-infrared) regime, for example, a CP light only carrying SAM, can also induce a transmission light with OAM of topological charge 1. In addition, we investigate the mechanism of how a Hankel-type (spiral) SPP is launched at the film's interface via a nanohole. We propose that the major cause is due to the conversion of a helical SPP of mode 1 creeping from the outlet of a nanohole into a Hankel-type SPP of order 1 at the film's surface. First, we theoretically characterize the SPPs of various modes propagating along an infinitely long metallic nanohole by solving a transcendental equation.[31−33] Comparing these modes, we think that a helical SPP of mode 1 is the dominant mode propagating along a metallic nanohole based on a consideration of the propagation length. Alternatively, we use a finite element method (FEM) to numerically investigate how a helical SPP converts into a spiral SPP at the outlet of a nanohole in a thick metal film; a schematic is plotted in Figure 1. This conversion of SPPs is via the edge of the outlet

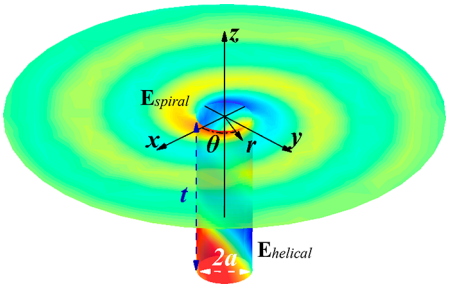

Figure 1. Schematic of a helical SPP propagating upward in a metallic nanohole converted into a spiral SPP outward propagating at the upper surface from the outlet, where a is the radius of nanohole, and t is the thickness of metal film. Cylindrical coordinates (r, θ, z) are used to describe the behaviors of these SPPs.

of a nanohole. Since SPP is a collective motion of free electrons in metal interacting with the electromagnetic (EM) field, the conversion is an extension of SPP creeping from the nanohole to the upper surface. In addition, the radiation of the energy flux of a helical SPP from the outlet of nanohole will be studied. The OAM carried by the transmission light will be identified by the phase singularity.[19−21,33] Moreover, the interferences of two spiral SPPs from a pair of nanoholes and multi-spiral SPPs from a 2D array of nanoholes will be studied.

METHOD

Throughout this paper, the time factor of the EM field is $\exp(-i\omega t)$, and the subscripts of 1 and 2 represent the surrounding dielectric medium and the metal, respectively. We assume a Bessel-type SPP of mode m inside the dielectric medium through an infinitely long circular nanohole with a radius of a. The electrical field of z component in terms of wavenumber β_m for an SPP of mode m in the dielectric medium passing through a nanohole is expressed in cylindrical coordinates (r, θ, z) as

$$E_{1z}(r, \theta, z) \propto J_m(r\sqrt{k_1^2 - \beta_m^2})\exp(\pm im\theta)\exp(i\beta_m z) \quad (1)$$

where J_m is the first-kind Bessel function of order m ($m = 0, \pm1, \pm2, \ldots$), $0 \le r \le a$, and $k_1 = 2\pi n/\lambda$. Here, λ is the wavelength of the incident light in vacuum, and n is the refractive index of the surrounding medium. eq 1 is derived in the cylindrical coordinates based on E_z satisfying a scalar Helmholtz equation in material 1. Similarly, the counterpart of eq 1 in the metal side $(a \le r)$ for an SPP of mode m is expressed as

$$E_{2z}(r, \theta, z) \propto H_m^{(1)}(r\sqrt{k_2^2 - \beta_m^2})\exp(\pm im\theta)\exp(i\beta_m z) \quad (2)$$

where $H_m^{(1)}$ is the first-kind Hankel function of order m, and $k_2 = 2\pi\sqrt{\varepsilon_{2r}}/\lambda$. Here, ε_{2r} is the relative permittivity of metal. Using eqs 1 and 2 satisfying $E_{1z}(a, \theta, z) = E_{2z}(a, \theta, z)$ and the other components of EM field matching the boundary conditions at the wall of nanohole, we can obtain a transcendental equation

$$\left(\frac{m\beta_m}{k_2^2 - \beta_m^2} - \frac{m\beta_m}{k_1^2 - \beta_m^2}\right)^2 = \left(\frac{k_1^2 a}{\sqrt{k_1^2 - \beta_m^2}}\frac{J_m'(a\sqrt{k_1^2 - \beta_m^2})}{J_m(a\sqrt{k_1^2 - \beta_m^2})} - \frac{k_2^2 a}{\sqrt{k_2^2 - \beta_m^2}}\frac{H_m^{(1)'}(a\sqrt{k_2^2 - \beta_m^2})}{H_m^{(1)}(a\sqrt{k_2^2 - \beta_m^2})}\right) \times \left(\frac{a}{\sqrt{k_1^2 - \beta_m^2}}\frac{J_m'(a\sqrt{k_1^2 - \beta_m^2})}{J_m(a\sqrt{k_1^2 - \beta_m^2})} - \frac{a}{\sqrt{k_2^2 - \beta_m^2}}\frac{H_m^{(1)'}(a\sqrt{k_2^2 - \beta_m^2})}{H_m^{(1)}(a\sqrt{k_2^2 - \beta_m^2})}\right) \quad (3)$$

where β_m is a complex wavenumber of the mode-m SPP.[32,33] We can calculate the dispersion relation of mode-m SPP in a nanohole by solving eq 3 numerically to find the complex root of β_m.[33] In particular, the behavior of the mode-1 SPP will be concerned due to its long propagation length in the following.

However, an analytical form of an outward-propagating Hankel-type (spiral) SPP of order m in the dielectric medium ($z \ge 0$) at a flat dielectric/metal interface can be expressed in cylindrical coordinates (r, θ, z) as

$$E_{1z}(r, \theta, z) \propto H_m^{(1)}(rk_{sp})\exp(\pm im\theta)\exp(i\sqrt{k_1^2 - k_{sp}^2}z) \quad (4)$$

where $\mathrm{Im}(\sqrt{k_1^2 - k_{sp}^2}) > 0$ and $k_{sp} = k_1\sqrt{\frac{\varepsilon_{2r}}{\varepsilon_{1r} + \varepsilon_{2r}}}$; $n = \sqrt{\varepsilon_{1r}}$. The counterpart of eq 4 inside metal ($z \le 0$) is

$$E_{2z}(r, \theta, z) \propto H_m^{(1)}(rk_{sp})\exp(\pm im\theta)\exp(-i\sqrt{k_2^2 - k_{sp}^2}z) \quad (5)$$

where $\mathrm{Im}(\sqrt{k_2^2 - k_{sp}^2}) > 0$. The propagation length of spiral SPP at interface is about $1/\mathrm{Im}(2k_{sp})$ with a wavelength of $2\pi/\mathrm{Re}(k_{sp})$. In the following study, we will focus on how a helical SPP in a nanohole converts into a spiral SPP at the interface. We believe that a natural way for a part of a helical SPP propagating in a nanohole to continue its polariton is to make a ninety-degree turn at the outlet edge and convert into a spiral SPP outward propagating at the interface of a thick film. We also apply FEM (COMSOL) to further verify this phenomenon for a thick metal film with a nanohole irradiated by a CP light.

https://doi.org/10.1021/acsomega.1c07187
ACS Omega 2022, 7, 10420−10428

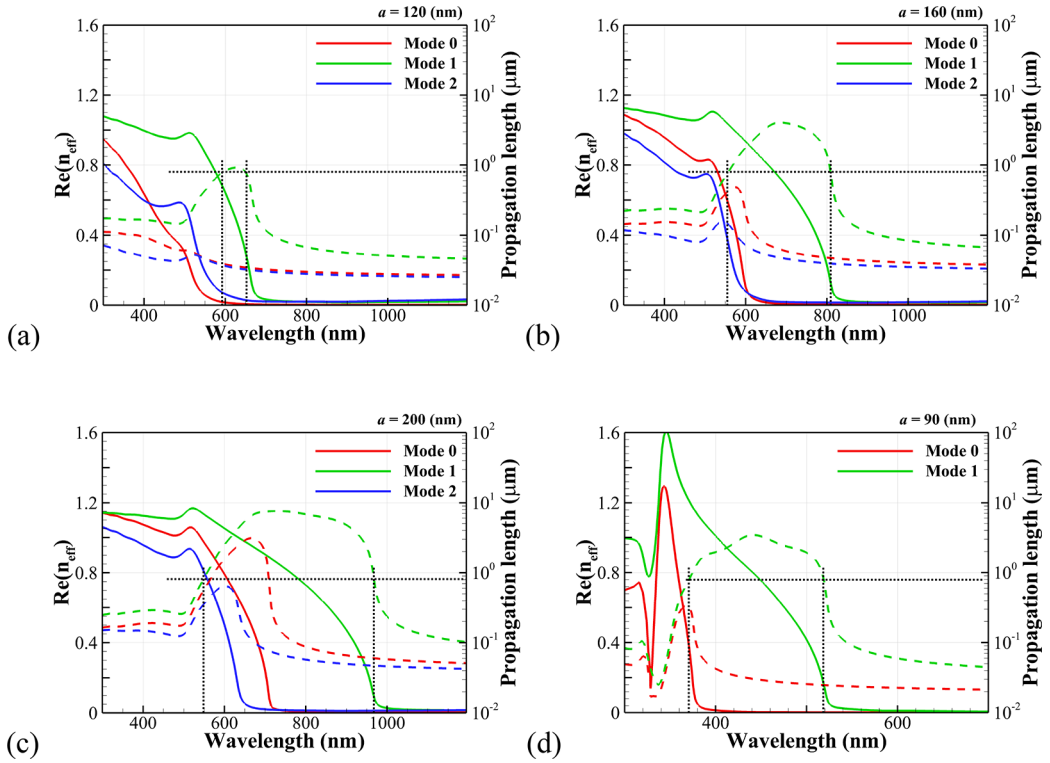

Figure 2. Dispersions of SPP of modes 0, 1, and 2 in a nanohole; Re(n_{eff}) and propagation length vs wavelength. Au film with a nanohole of (a) a = 120 nm, (b) a = 160 nm, and (c) a = 200 nm. (d) Ag film with a nanohole of a = 90 nm. Solid lines: wavenumber of Re(n_{eff}), and dash lines: propagation length (R: 0, G: 1, B: 2 mode). Dot lines: bandpass region of propagation length according to a threshold of 800 nm.

RESULTS AND DISCUSSION

In the following, we do not take the substrate effect into account. Therefore, an effective refractive index of the surrounding medium is assumed to be 1.2, throughout this paper, to simulate a real case: a metal film on a silica substrate immersed in air. First, we numerically calculate the dispersion relation of SPP of different modes (m = 0, 1, 2) in an infinite nanohole from the complex root β_m of transcendental equation, eq 3.[33,34] Dielectric constants of Au and Ag measured by Johnson and Christy are used for simulation.[35] The Re(n_{eff}) and propagation length 1/Im($2\beta_m$) versus wavelength for different-size nanoholes in Au or Ag thick film are plotted in Figure 2, where the effective refractive index is defined as $n_{eff} = \beta_m/k_0$. These spectra of propagation length indicate that a specific-sized nanohole is a bandpass filter. In particular, the propagation length of an SPP of mode 1 is much larger than the other modes in a specific frequency band, which is size-dependent. This is to say that only the wavelength-selective SPP of mode 1 is allowed to pass through a nanohole of specified size in a thick metal film. In general, the larger the nanohole's radius the more red-shifted and broadened the bandpass region of the propagation length of mode-1 SPP. Since the thicknesses of most metal films are thinner than 400 nm, a typical length of 800 nm is chosen as the threshold for the propagation length to define the bandpass region and bandwidth of each mode. If the threshold of propagation length is 800 nm (dot line in Figure 2), the bandpass region of mode-1 SPP is [595, 650] for a = 120 nm, [560, 810] nm for a = 160 nm, and [548, 968] nm for a = 200 nm in Au film. For a nanohole of a = 90 nm in Ag film, the bandpass region of mode-1 SPP is [370, 520] nm (Figure 2d). In addition, the propagation length of mode-1 SPP increases as the size of the nanohole increases. This could be attributed to the attenuation of SPP along nanohole being mainly due to the confinement of the metal wall and the induced Ohm loss. If the diameter of the nanohole is larger, the attenuation is less, so the propagation length is larger. Note that, for a bigger nanohole of a = 200 nm in Au film, as shown in Figure 2c, the propagation length of mode-0 SPP is also larger than 800 nm in a bandpass region of 565−709 nm. For this case, not only mode-1 SPP but also mode-0 SPP can propagate through the nanohole in a thick gold film of 1 μm. The bandpass region of the propagation length of SPP is mode-dependent. Generally, the lower cutoff wavelength of the bandpass region depends on the plasmon property of metal, and the upper cutoff wavelength depends on the size of nanohole as well as the refractive index of surrounding medium.

In addition, Figure 3a shows the streamlines of a Poynting vector (energy flux) $\mathbf{S} = \mathrm{Re}(\mathbf{E} \times \bar{\mathbf{H}})/2$ of the mode-1 SPP within a nanohole of a = 160 nm in Au film at λ = 700 nm, which is within the bandpass region of Figure 2b; $n_{eff} = 0.6810 + 1.3965 \times 10^{-2}i$. The corresponding propagation length is 3.99 μm. Figure 3a shows the phase front of the surface charge, Re(D_n), of Bessel-type SPP of mode 1 (eq 1) on the metal wall of a nanohole at λ = 700 nm, where $D_n = \varepsilon_{1r}\varepsilon_0\mathbf{E}\cdot\mathbf{n}$. The helix angle is $\phi = 45.64°$ according to $\tan(\phi) = m/\mathrm{Re}(\beta_m a)$. The pitch of the helix is the wavelength of SPP; λ_{sp} = 1029 nm. Additionally, the direction of the streamline of the Poynting vector (energy flux) $\mathbf{S}$ on the wall is perpendicular to the phase front (Figure 3a). Note that, for this case, the phase velocity of a helical SPP of m = 1 is larger than light speed in vacuum. This is similar to the case of an opaquely incident plane wave encountering a planar interface; the phase velocity along the interface is larger than light speed. However, the group velocity of SPP is still slower than light speed. The spatial phase distribution of E_z in a nanohole shows a phase singularity with topological charge of 1 (eq 1). The

https://doi.org/10.1021/acsomega.1c07187
ACS Omega 2022, 7, 10420−10428

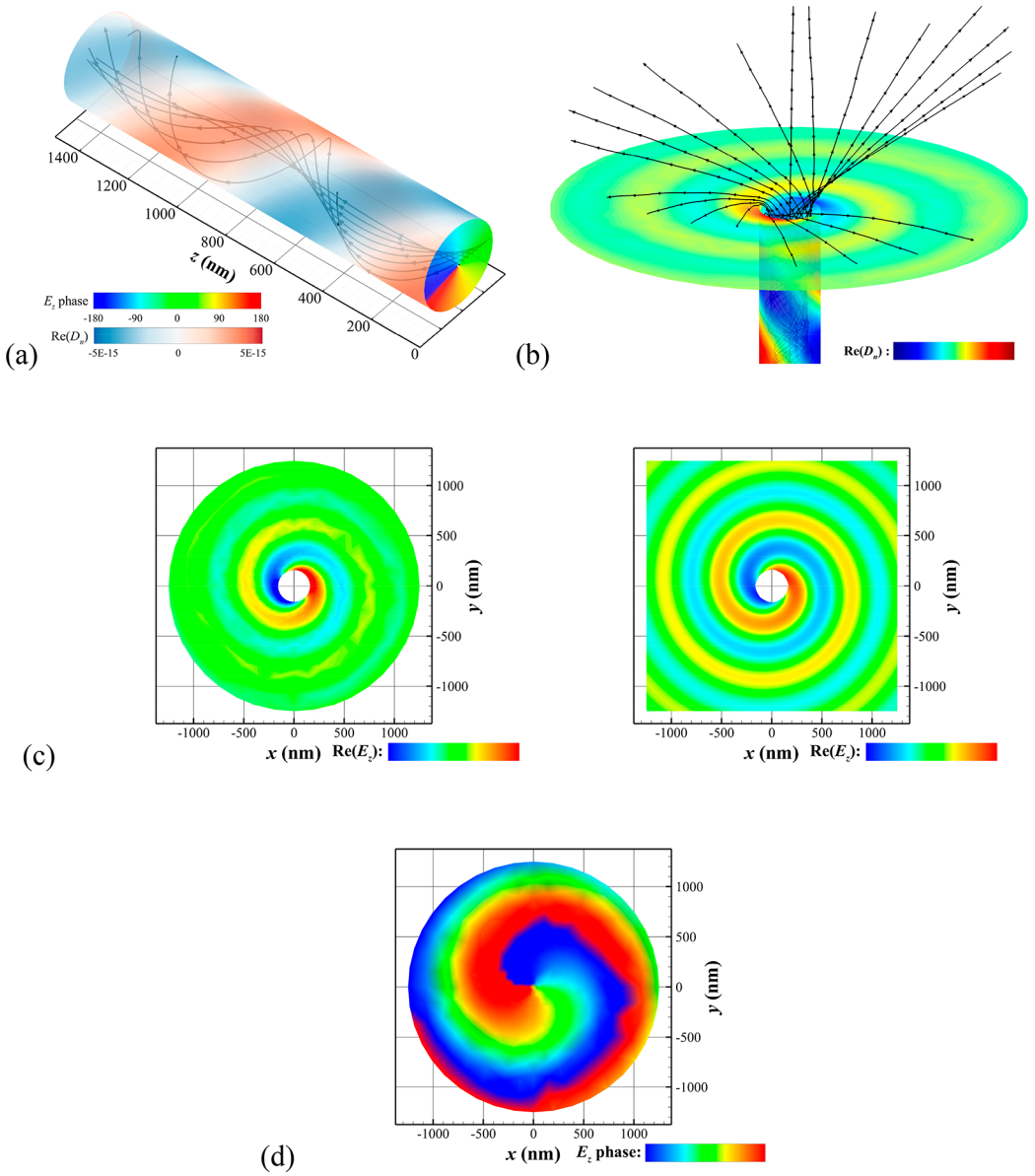

Figure 3. (a) The streamlines of energy flux of mode-1 SPP in a nanohole of a = 160 nm and the phase front of surface charge Re(D_n) on the wall of nanohole in Au film at λ = 700 nm (analytical solution). (b) The streamlines of energy flux and the phase fronts of Re(D_n) on the nanohole's wall and at the upper interface, induced by a CP plane wave of λ = 700 nm incident normally on 1 μm Au film (FEM results). (c) LHS: FEM result of Re(E_z) at the upper interface (z = 0) showing outward-propagating spiral SPP, and RHS: analytical form of Hankel-type SPP at the interface. (d) Spatial phase distribution of E_z field at z = 1500 nm, indicating a phase singularity with a topological charge of 1.

winding behavior of streamline of energy flux and the phase singularity of the optical field are indications of an optical vortex carrying OAM.[33,36] Furthermore, the full-field responses of an incident CP plane wave, $\mathbf{E}^i = e^{ik_1 z}(\mathbf{e}_x + i\mathbf{e}_y)/\sqrt{2}$, irradiating a thick metal film with a single nanohole, are analyzed by FEM (COMSOL) numerically, where the thickness of the film is 1 μm, as shown in Figure 3b. Since the thickness of the metal film is larger than the penetration depth of a normally incident light in metal, the only way for light to transmit is via the nanohole. In addition, the crosstalk of SPPs on both sides of the metal film will not happen. Figure 3b shows that the phase front of Re(D_n) on the wall of the nanohole in a finite-thickness film has a pitch of 1028 and a helix angle of 46°, which are consistent with the results of an analytical solution of a mode-1 SPP (Figure 3a). It illustrates that the induced SPP by CP light, propagating along a nanohole in a finite-thickness film, is a mode-1 SPP. Figure 3b also indicates that the streamline of energy flux of the mode-1 SPP fans out toward the medium at the outlet of the nanohole. In addition, part of the energy flow creeps along the metallic wall and makes a turn at the edge of the outlet to convert into a spiral (Hankel type of order 1) SPP propagating outward from the nanohole at the interface of film and dielectric medium. According to eq 4, the analytical form of an outward propagating spiral SPP of order 1 at the interface ($z \geq 0$) is expressed as

$$E_{1z}(r, \theta, z) = E_0 H_1^{(1)}(rk_{sp})\exp(i\theta)\exp(i\sqrt{k_1^2 - k_{sp}^2}z) \quad (6)$$

where the complex amplitude E_0 depends on the film thickness, diameter, refractive index of medium, and wavelength. We can use the result of FEM to fit eq 6 for obtaining appropriate E_0. Figure 3c shows that the patterns of phase front, Re(E_z), at z = 0 of FEM result (left-hand side, LHS) and the analytical solution

https://doi.org/10.1021/acsomega.1c07187
ACS Omega 2022, 7, 10420−10428

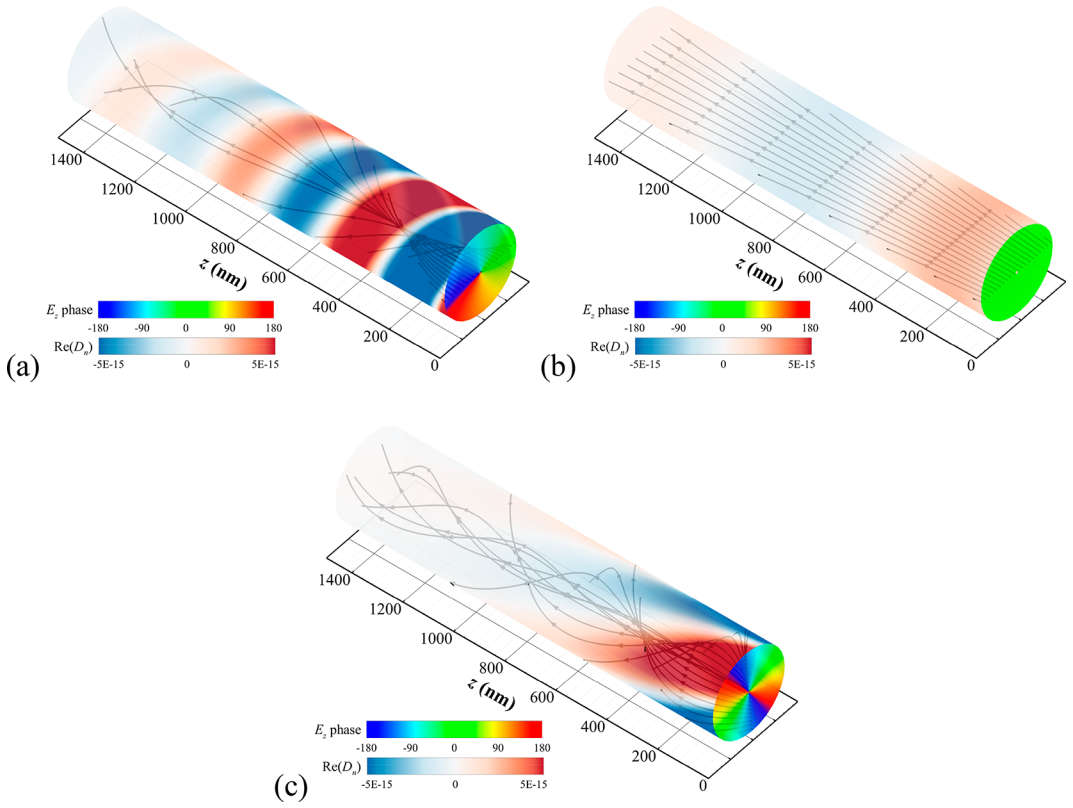

Figure 4. Streamlines of energy flux (analytical solution) in a nanohole of a = 160 nm and the phase front of the surface charge Re(D_n) on the wall of a nanohole in Au film of infinite thickness. (a) Mode-1 SPP at λ = 500 nm, (b) mode-0 SPP at λ = 570 nm, and (c) mode-2 SPP at λ = 550 nm. Phase distribution of E_z at a cross section of a nanohole for each mode indicates the corresponding topological charge.

of eq 6 (right-hand side, RHS). Both phase fronts are almost identical; the pattern of Re(E_z) exhibits a spiral phase front of this spiral SPP. This demonstrates that the new generated SPP at the upper interface is an outward-propagating Hankel-type SPP of order 1 with λ_{sp} = 557 nm at λ = 700 nm; $k_{sp} = k_1\sqrt{\frac{\varepsilon_{2r}}{\varepsilon_{1r}+\varepsilon_{2r}}}$. We also can observe that the streamlines of energy flux of this spiral (Hankel type of order 1) SPP are perpendicular to the phase front. Additionally, the spatial phase distribution of the E_z field at a cross section above the outlet (z = 1500 nm) is plotted in Figure 3d. The phase singularity with a topological charge of 1 is observed, which is evidence of the transmission light from the nanohole's outlet carrying OAM. In summary, these results elucidate that a plasmonic nanohole is a bandpass filter of selecting mode-1 SPP with OAM to pass through, as a CP plane wave is incident. Furthermore, a part of the transmission SPP converts into a spiral (Hankel type) SPP outward propagating at the upper interface.

If the frequency of incident light is not within the bandpass region of mode-1 SPP, the propagation length of the induced SPP is short. For example, the streamlines of Poynting vector and phase fronts of the surface charge Re(D_n) of mode-1 SPP at λ = 500 and 900 nm are shown in Figure 4a and Figure S1 (Supporting Information), respectively (analytical solution). As for the SPPs of the other modes (m = 0, 2) within a nanohole of a = 160 nm in Au film, the results of mode-0 SPP at λ = 570 nm and mode-2 SPP at λ = 550 nm are shown in Figure 4b,c. These profiles demonstrate that this energy flux of an SPP is attenuated rapidly, not allowed to tunnel through the nanohole. Additionally, the streamlines of energy flux of mode-0 SPP exhibit straight lines, rather than helical lines (Figure 4b). Except the mode 0, the higher-order SPPs exhibit helical propagation in a nanohole; the phase fronts of SPPs of modes 1 and 2 on the metal wall also exhibit helical distributions. The spatial phase distribution of E_z at a cross section of a nanohole for each mode is also plotted in Figure 4 to indicate the corresponding topological charge. For example, Figure 4b indicates the topological charge is 2 for mode-2 SPP.

As for Ag film, the results in a nanohole are shown in Figure 5. Figure 5a shows the streamlines of the Poynting vector of mode-1 SPP and the phase front of Re(D_n) on the wall of a nanohole (a = 90 nm) in Ag film at λ = 440 nm in a medium of n = 1.2; the phase of E_z at the cross section indicates the topological charge of 1. According to eq 3, the wavenumber is β_1 = 11.4882 + 0.1461i μm^{-1}. The propagation length of helical mode-1 SPP is 3.42 μm at λ = 440 nm within the bandpass region of a nanohole in Ag film, as shown in Figure 2d. The pitch, λ_{sp}, of the helix of phase front, Re(D_n), is 547 nm, and the helix angle ϕ is 44.05°. Again, we observe that the streamline of the Poynting vector on the wall is perpendicular to the phase front. Figure 5b–d shows the results calculated by FEM for a nanohole in Ag film with thickness of 1 μm, irradiated by a CP light. Again, Figure 5b illustrates that the streamlines of energy flux spread with a large divergence angle at the outlet of a nanohole. A standing wave in the nanohole is observed (Figure 5c), which is the result of a reflected mode-1 SPP from the outlet interfering with the upward propagating SPP. For this case, the thickness of Ag film nearly satisfies the resonance condition of mode-1 SPP if the thickness is an integer multiple of λ_{sp}. Therefore, the pattern of nodal line of |**E**| is clearer, as shown in Figure 5c (RHS). Additionally, the distribution of Re(E_z) on the wall (LHS) is also plotted to show the helical SPP. The corresponding Re(E_z) at

https://doi.org/10.1021/acsomega.1c07187
ACS Omega 2022, 7, 10420−10428

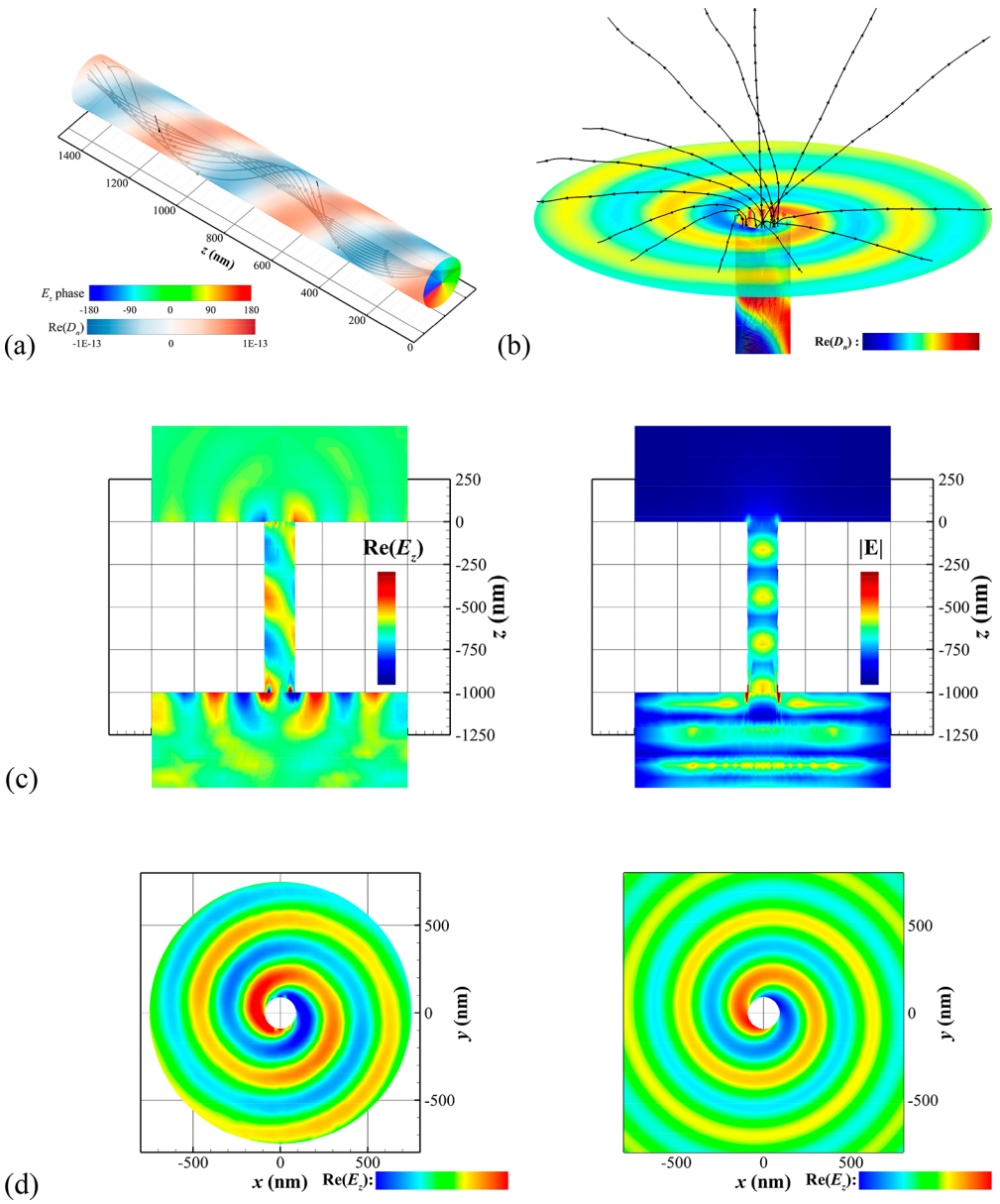

Figure 5. In Ag film, mode-1 SPP passing through a nanohole of $a = 90$ nm at $\lambda = 440$ nm. (a) The streamlines of energy flux inside an infinite nanohole and $\mathrm{Re}(D_n)$ on the wall (analytical solution). (b) The streamlines of energy flux at the outlet. (c) The intensities of $\mathrm{Re}(E_z)$ on the wall and $|\mathbf{E}|$ at the x-z cross section of $y = 0$ inside a nanohole in Ag film with a finite thickness of $t = 1$ μm, induced by an incident CP plane wave (FEM results). LHS: $\mathrm{Re}(E_z)$, and RHS: $|\mathbf{E}|$. (d) The corresponding $\mathrm{Re}(E_z)$ at the interface of film ($z = 0$). LHS: FEM, and RHS: Hankel-type SPP of order 1.

the interface of Ag film ($z = 0$), calculated by FEM, is shown in LHS of Figure 5d, and the analytical solution of Hankel SPP of order 1 is shown in RHS. By a comparison of both spiral phase fronts, we conclude that the induced SPP is a Hankel SPP of order 1. It is originated from the conversion of the creeping mode-1 SPP on the wall of a nanohole.

If the incident light illuminating metal film with a nanohole is an LP light, two helical mode-1 SPPs with right-handedness and left-handedness are induced in the nanohole. This is because an LP light is the linear superposition of right-handed and left-handed CP lights. Therefore, two spiral SPPs with opposite handedness are generated from the nanohole's outlet at the backside interface; they combine together to become a Hankel-type SPP of mode 1 in the medium ($z \geq 0$).

$$E_{1z}(r, \theta, z) \propto H_1^{(1)}(rk_{sp})\cos(\theta)\exp(i\sqrt{k_1^2 - k_{sp}^2}\,z) \qquad (7)$$

Moreover, we study the interference of two SPPs originating from a pair of nanoholes of $a = 160$ nm with a pitch (center to center) of 620 nm in Au film of $t = 1$ μm. The phase front $\mathrm{Re}(E_z)$ of FEM and an approximation of the superposition of two Hankel-type SPPs of order 1, eq 6, individually originating from the two nanoholes at interface of $z = 0$ are shown in Figure 6 for comparison, where a right circularly polarized (RCP) light of $\lambda = 700$ nm irradiates the film from the lower side. We found that the result of the approximation is in agreement with that of FEM. Using this approximation, the pitch between two nanoholes can be easily optimized to tailor the interference of two Hankel-type SPPs for a constructive or destructive purpose.

We also use FEM with a periodic boundary condition to simulate the interference of multi SPPs from a 2D nanohole array ($a = 160$ nm) with a pitch of 1000 nm (lattice constant) in Au film irradiated by a CP light of $\lambda = 700$ nm. The $\mathrm{R}(E_z)$

https://doi.org/10.1021/acsomega.1c07187
ACS Omega 2022, 7, 10420−10428

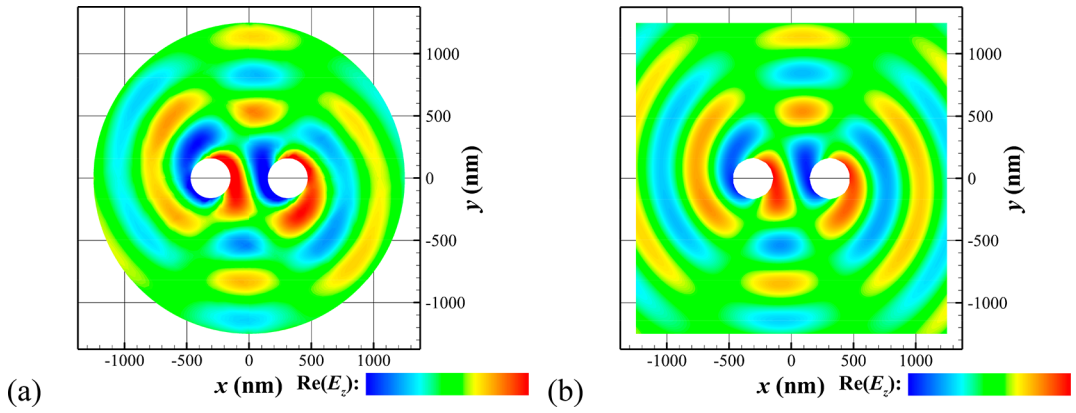

Figure 6. Interference of SPPs at the upper side ($z = 0$) originating from two nanoholes of $a = 160$ nm with $p = 620$ nm in Au film of $t = 1$ μm, irradiated by an RCP plane wave of $\lambda = 700$ nm at the lower side ($z = -t$). Re(E_z) of (a) FEM and (b) approximation of the sum of two Hankel-type SPPs of order 1 at the upper interface of $z = 0$.

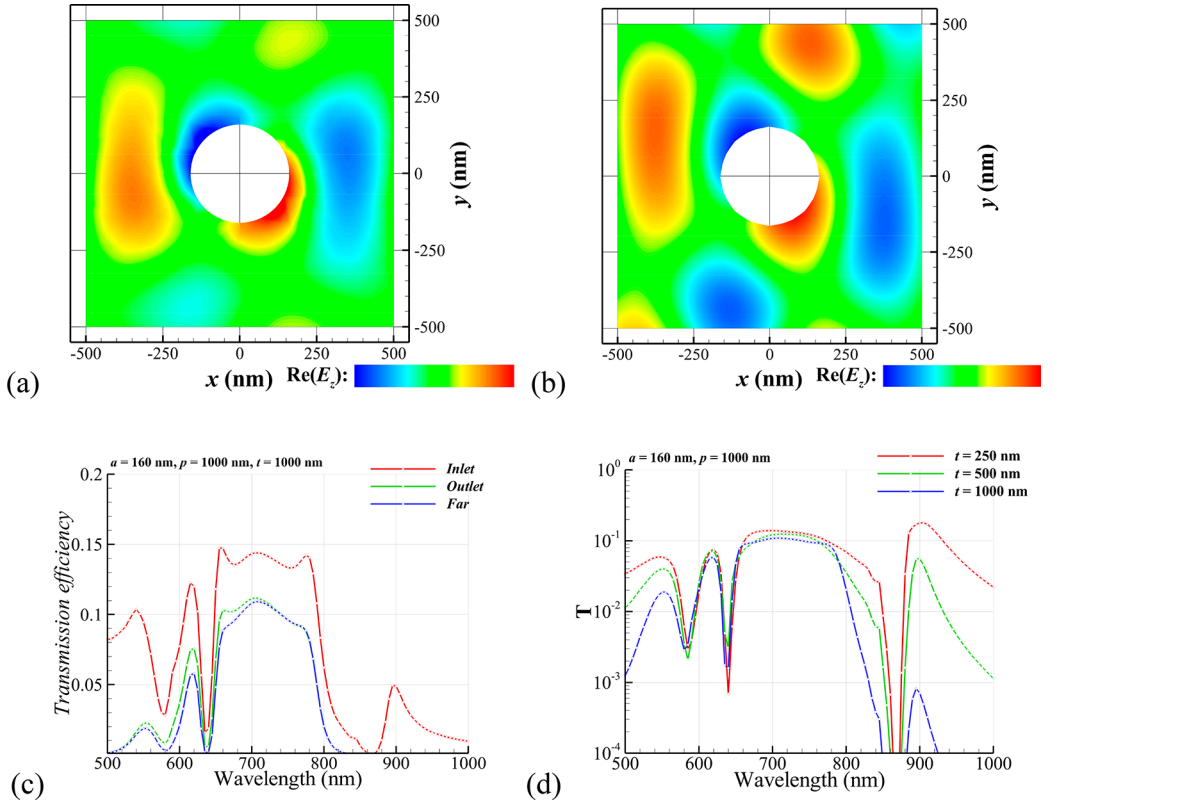

Figure 7. 2D nanohole array of $a = 160$ nm and $p = 1000$ nm (lattice constant) in Au film with $t = 1$ μm irradiated by an RCP plane wave of $\lambda = 700$ nm at the lower interface ($z = -t$). The Re(E_z) calculated by (a) FEM with a periodic boundary condition and (b) by an approximation of a 5 × 5 array of Hankel-type SPPs at the interface of $z = 0$. (c) Spectra of transmission efficiencies at the inlet, outlet, and far field of a nanohole. (d) Spectrum of transmission efficiency T of a nanohole array in Au films of different thicknesses: $t = 250$, 500, 1000 nm.

calculated by FEM at the interface of $z = 0$ and by an approximation of Hankel SPPs of order 1 originating from a 5 × 5 array are plotted in Figure 7. Again, we found that the result of the approximation of Hankel SPPs is in agreement with that of FEM, in comparison of Figure 7a,b. Figure 7c shows the FEM result of the spectrum of transmission efficiencies at the inlet, outlet, and far field of a nanohole array in Au films with $t = 1000$ nm and $p = 1000$ nm. The transmission efficiency T_I at the inlet ($z = -t$) or T_O at the outlet ($z = 0$) is defined as

$$T_{IO} = \frac{\int_A \mathbf{S}\cdot\mathbf{e}_z \, dA}{\int_{A_0} \mathbf{S}_0\cdot\mathbf{e}_z \, dA} \tag{8}$$

where A is the area of a nanohole, A_0 is the area of a unit cell, and $\mathbf{S}_0$ is the Poynting vector of incident light. As for the transmission efficiency T at the far field, the area for the integral of the numerator in eq 8 is A_0, a unit cell of array ($p \times p$), at $z = 1000$ nm. The bandpass region of transmission efficiency (Figure 7c) is consistent with that of the propagation length of mode-1 SPP (Figure 2b for $a = 160$ nm); the bandpass region is from 580 to 800 nm for a threshold of 1 μm propagation length. However,

https://doi.org/10.1021/acsomega.1c07187
ACS Omega 2022, 7, 10420−10428

there is an obvious dip in this band at λ = 637 nm for T_I, as shown in Figure 7c. This dip corresponds to a band rejection of the incident energy flux flowing into a nanohole array of p = 1000 nm, that is, a strong reflection. Generally, the wavelengths of dip mainly depend on the pitch of array. According to Bloch's equation

$$\frac{2\pi l}{p}\sqrt{i^2 + j^2} = \mathrm{Re}(k_{sp}) \tag{9}$$

the estimated wavelengths λ of dip are 586 nm (i = 2, j = 1, l = 1), 638 nm (i = 1, j = 0, l = 2), and 870 nm (i = 1, j = 1, l = 1).[3,37] These values are in agreement with those calculated by FEM; 582, 637, and 866 nm. For different pitches (p = 1000, 1100, 1200 nm), the transmission efficiencies T are shown in Figure S2 and Table S1 (Supporting Information). Our results show that the wavelengths of dip calculated by FEM are in agreement with those estimated by eq 9. Figure 7c also illustrates that the transmission efficiency at the outlet (z = 0) is less than that at the inlet ($z = -t$) due to the attenuation of mode-1 SPP in a nanohole; $T_O \leq T_I$. Additionally, the transmission efficiency T at the far field is less than that at the outlet (z = 0) due to the partial energy of mode-1 SPP being converted into a Hankel-type SPP at the interface (z = 0); $T \leq T_O$. We also investigate the thickness effect of film on the transmission. The results for Au film of different thicknesses (t = 250, 500, 1000 nm) with a nanohole of a = 160 nm and p = 1000 nm are shown in Figure 7d. From these spectra of transmission efficiency T, we found that the bandpass region and the dip are nearly independent of the thickness of Au film for the same pitch, except that the thicker the film the smaller the transmission efficiency. Moreover, we can adjust the pitch of a nanohole array to control the constructive or destructive interference of multi SPPs. For example, through suppressing the interference of multi SPPs of a 2D nanohole array the coherent emission from multi nanoholes at the far field becomes possible.[8,38] Conversely, a coherent resonance of SPPs could be achieved by a specific design for the pattern of nanoholes.[39]

CONCLUSION

From the dispersion relations of SPPs of different modes propagating along a metallic nanohole solved by a transcendental equation, we found that the propagation length of mode-1 SPP is much larger than that of the other modes in a size-dependent frequency band. In this band region, the streamlines of energy flux (Poynting vector) of a mode-1 Bessel-type SPP in the nanohole exhibit helixes carrying OAM. The distribution of $\mathrm{Re}(D_n)$ on the wall of a nanohole shows the phase front of the helical SPP with a helix angle; the streamline of energy flux is perpendicular to this phase front. A coil-shaped helical SPP of mode 1 might be a natural way for light to propagate through a sub-wavelength nanohole in metal film. Furthermore, numerical results of a thick Au or Ag film show that, if an incident CP light is used for illumination, only the mode-1 SPP is allowed to reach the outlet. Additionally, most of the energy flux of mode-1 SPP fans out as a radiating dipole source at the outlet of a nanohole carrying OAM with a topological charge of 1. Of interest, when a mode-1 helical SPP creeps out of the nanohole's outlet a part of it converts into a spiral (Hankel type of order 1) SPP outward propagating at the metal−dielectric interface of the film; their handedness is the same. If an incident LP light is used for illumination, two helical SPPs with opposite handedness are generated simultaneously to propagate along a nanohole. This is because an LP light can be decomposed into right-handed and left-handed CP lights. Consequently, a total SPP of two spiral SPPs with opposite handedness is induced at the outlet of a nanohole to propagate at the interface. We also studied the interference of two spiral SPPs generated from two nanoholes and the interference of multi spiral SPPs from a 2D nanohole array. We found that the results of an approximation solution in terms of Hankel form are in agreement with those of FEM. Our studies may provide an insight into the mechanism of interference of multi spiral SPPs converted from the transmission helical SPPs via a metallic nanohole array. These findings will be useful to design nanohole-array metamaterials for applying SPP to nearfield sensing, for example, Fano resonance.[6,9,40−43] In addition, it is worth mentioning that a higher-order SPP with a topological charge larger than 1 could be generated efficiently through nanoholes in a plasmonic film by using a special structured-light (e.g., Bessel beam) irradiation.

ASSOCIATED CONTENT

Supporting Information

The Supporting Information is available free of charge at https://pubs.acs.org/doi/10.1021/acsomega.1c07187.

Electric fields of analytical form in cylindrical coordinates; fields distribution of mode-1 SPP with wavelength outside bandpass region; dip of transmission spectrum based on Bloch's theorem (PDF)

AUTHOR INFORMATION

Corresponding Authors

Jiunn-Woei Liaw − *Department of Mechanical Engineering, Chang Gung University, Kwei-Shan, Taoyuan 333, Taiwan; Department of Mechanical Engineering, Ming Chi University of Technology, New Taipei City 243303, Taiwan; Proton and Radiation Therapy Center, Linkou Chang Gung Memorial Hospital, Taoyuan City 33305, Taiwan;* orcid.org/0000-0003-0179-5274; Email: markliaw@mail.cgu.edu.tw

Mao-Kuen Kuo − *Institute of Applied Mechanics, National Taiwan University, Taipei 106, Taiwan;* orcid.org/0000-0003-0524-8227; Email: mkkuo@ntu.edu.tw

Authors

Yun-Cheng Ku − *Institute of Applied Mechanics, National Taiwan University, Taipei 106, Taiwan*

Szu-Yao Mao − *Institute of Applied Mechanics, National Taiwan University, Taipei 106, Taiwan*

Complete contact information is available at: https://pubs.acs.org/10.1021/acsomega.1c07187

Author Contributions

J.W.L. proposed the initial idea and designed the research together with M.K.K.; Y.C.K. performed the simulations and data analysis. S.Y.M. assisted in finding complex roots of analytical solution. J.W.L., M.K.K., and Y.C.K. wrote the manuscript through contributions of all authors. All authors have given approval to the final version of the manuscript.

Notes

The authors declare no competing financial interest.

ACKNOWLEDGMENTS

The research was supported by Ministry of Science and Technology, Taiwan (MOST 110-2221-E-182-039-MY3, 110-

2221-E-002-151) and Chang Gung Memorial Hospital (CIRPD2I0023).

REFERENCES

(1) Ebbesen, T. W.; Lezec, H. J.; Ghaemi, H. F.; Thio, T.; Wolff, P. A. Extraordinary optical transmission through sub-wavelength hole arrays. *Nature* **1998**, *391*, 667−669.
(2) Barnes, W. L.; Dereux, A.; Ebbesen, T. W. Surface plasmon subwavelength optics. *Nature* **2003**, *424*, 824−830.
(3) Barnes, W. L.; Murray, W. A.; Dintinger, J.; Devaux, E.; Ebbesen, T. W. Surface plasmon polaritons and their role in the enhanced transmission of light through periodic arrays of subwavelength holes in a metal film. *Phys. Rev. Lett.* **2004**, *92*, 107401.
(4) Laluet, J.-Y.; Devaux, E.; Genet, C.; Ebbesen, T. W.; Weeber, J.-C.; Dereux, A. Optimization of surface plasmons launching from subwavelength hole arrays: modelling and experiments. *Opt. Express* **2007**, *15*, 3488−3495.
(5) Du, B.; Ruan, Y.; Yang, D.; Jia, P.; Gao, S.; Wang, Y.; Wang, P.; Ebendorff-Heidepriem, H. Freestanding metal nanohole array for high-performance applications. *Photon. Res.* **2020**, *8* (11), 1749−1756.
(6) Kang, E. S. H.; Ekinge, H.; Jonsson, M. P. Plasmonic fanoholes: on the gradual transition from suppressed to enhanced optical transmission through nanohole arrays in metal films of increasing film thickness. *Opt. Mater. Express* **2019**, *9*, 1404−1414.
(7) Wu, L.; Bai, P.; Li, E. P. Designing surface plasmon resonance of subwavelength hole arrays by studying absorption. *J. Opt. Soc. Am. B* **2012**, *29* (4), 521−528.
(8) Gao, H.; Hyun, J. K.; Lee, M. H.; Yang, J.-C.; Lauhon, L. J.; Odom, T. W. Broadband plasmonic microlenses based on patches of nanoholes. *Nano Lett.* **2010**, *10*, 4111−4116.
(9) Nishida, M.; Hatakenaka, N.; Kadoya, Y. Multipole surface plasmons in metallic nanohole arrays. *Phys. Rev. B* **2015**, *91*, 235406.
(10) Muller, R.; Malyarchuk, V.; Lienau, C. Three-dimensional theory on light-induced near-field dynamics in a metal film with a periodic array of nanoholes. *Phys. Rev. B* **2003**, *68*, 205415.
(11) Lezec, H. J.; Thio, T. Diffracted evanescent wave model for enhanced and suppressed optical transmission through subwavelength hole arrays. *Opt. Express* **2004**, *12* (16), 3629−3651.
(12) de León-Pérez, F.; Brucoli, G.; García-Vidal, F. J.; Martín-Moreno, L. Theory on the scattering of light and surface plasmon polaritons by arrays of holes and dimples in a metal film. *New J. Phys.* **2008**, *10*, 105017.
(13) Alegret, J.; Johansson, P.; Käll, M. Green's tensor calculations of plasmon resonances of single holes and hole pairs in thin gold films. *New J. Phys.* **2008**, *10*, 105004.
(14) Müller, R.; Ropers, C.; Lienau, C. Femtosecond light pulse propagation through metallic nanohole arrays: The role of the dielectric substrate. *Opt. Express* **2004**, *12*, 5067−5081.
(15) Chen, C.-M.; Ke, J.-L.; Lan, Y.-C.; Chan, M.-C. Spiral surface plasmon modes inside metallic nanoholes. *Opt. Express* **2015**, *23*, 29321−29330.
(16) Shin, H.; Catrysse, P. B.; Fan, S. Effect of the plasmonic dispersion relation on the transmission properties of subwavelength cylindrical holes. *Phys. Rev. B* **2005**, *72* (8), 085436.
(17) Yin, L.; Vlasko-Vlasov, V. K.; Rydh, A.; Pearson, J.; Welp, U.; Chang, S.-H.; Gray, S. K.; Schatz, G. C.; Brown, D. E.; Kimball, C. W. Surface plasmons at single nanoholes in Au films. *Appl. Phys. Lett.* **2004**, *85*, 467−469.
(18) Chang, S.-H.; Gray, S. K.; Schatz, G. C. Surface plasmon generation and light transmission by isolated nanoholes and arrays of nanoholes in thin metal films. *Opt. Express* **2005**, *13*, 3150−3165.
(19) Nikitin, A. Y.; Garcıa-Vidal, F. J.; Martın-Moreno, L. Surface electromagnetic field radiated by a subwavelength hole in a metal film. *Phys. Rev. Lett.* **2010**, *105*, 073902.
(20) Häfele, V.; de Leon-Perez, F.; Hohenau, A.; Martın-Moreno, L.; Plank, H.; Krenn, J. R.; Leitner, A. Interference of surface plasmon polaritons excited at hole pairs in thin gold films. *Appl. Phys. Lett.* **2012**, *101*, 201102.
(21) Janipour, M.; Pakizeh, T.; Hodjat-Kashani, F. Optical interaction of a pair of nanoholes in Au film via surface plasmon polaritons. *IEEE Photonics J.* **2014**, *6*, 4800913.
(22) van Oosten, D.; Spasenovic, M.; Kuipers, L. Nanohole chains for directional and localized surface plasmon excitation. *Nano Lett.* **2010**, *10*, 286−290.
(23) Dikken, D. J. W.; Korterik, J. P.; Segerink, F. B.; Herek, J. L.; Prangsma, J. C. A phased antenna array for surface plasmons. *Sci. Rep.* **2016**, *6*, 25037.
(24) Gao, H.; Henzie, J.; Odom, T. W. Direct evidence for surface plasmon-mediated enhanced light transmission through metallic nanohole arrays. *Nano Lett.* **2006**, *6*, 2104−2108.
(25) Alaverdyan, Y.; Sepúlveda, B.; Eurenius, L.; Olsson, E.; Käll, M. Optical antennas based on coupled nanoholes in thin metal films. *Nat. Phys.* **2007**, *3*, 884−889.
(26) Nerkararyan, S.; Nerkararyan, Kh.; Janunts, N.; Pertsch, T. Generation of Hankel-type surface plasmon polaritons in the vicinity of a metallic nanohole. *Phys. Rev. B* **2010**, *82*, 245405.
(27) Tekkozyan, V. A. Surface plasmon-polaritons wave fields in the vicinity of a metallic nanohole. *J. Contemporary Phys. (Armenian Academy of Sciences)* **2013**, *48* (5), 214−219.
(28) Vuong, L. T.; Adam, A. J. L.; Brok, J. M.; Planken, P. C. M.; Urbach, H. P. Electromagnetic spin-orbit interactions via scattering of subwavelength apertures. *Phys. Rev. Lett.* **2010**, *104*, 083903.
(29) Wei, D.; Wang, Y.; Liu, D.; Zhu, Y.; Zhong, W.; Fang, X.; Zhang, Y.; Xiao, M. Simple and nondestructive on-chip detection of optical orbital angular momentum through a single plasmonic nanohole. *ACS Photonics* **2017**, *4*, 996−1002.
(30) Hua, D.-J.; Liu, Y.; Zhang, Z.-Y.; Xiao, X.; Du, J.-L. Angular-momentum-dependent splitting of light through metal nanohole. Proc. SPIE 9272, Optical Design and Testing VI, 92721J (November 6, 2014); SPIE, 2015 DOI: 10.1117/12.2073327.
(31) Stratton, A. *Electromagnetic theory;* McGraw-Hill: New York, 1941.
(32) Pfeiffer, C. A.; Economou, E. N.; Ngai, K. L. Surface polaritons in a circularly cylindrical interface: Surface plasmons. *Phys. Rev. B* **1974**, *10*, 3038−3051.
(33) Liaw, J.-W.; Mao, S.-Y.; Luo, J.-Y.; Ku, Y.-C.; Kuo, M.-K. Surface plasmon polaritons of higher-order mode and standing waves in metallic nanowires. *Opt. Express* **2021**, *29* (12), 18876−18888.
(34) Liaw, J.-W.; Wu, P.-T. Dispersion relation of surface plasmon wave propagating along a curved metal-dielectric interface. *Opt. Express* **2008**, *16*, 4945−4951.
(35) Johnson, P. B.; Christy, R. W. Optical constants of the noble metals. *Phys. Rev. B* **1972**, *6*, 4370−4379.
(36) Ku, Y. C.; Kuo, M. K.; Liaw, J. W. Winding Poynting vector of light around plasmonic nanostructure. *J. Quant. Spectrosc. Radiat. Transfer* **2022**, *278*, 108005.
(37) Liu, H.-W.; Lin, F.-C.; Lin, S.-W.; Wu, J.-Y.; Chou, B.-T.; Lai, K.-J.; Lin, S.-D.; Huang, J.-S. Single-crystalline aluminum nanostructures on a semiconducting GaAs substrate for ultraviolet to near-infrared plasmonics. *ACS Nano* **2015**, *9* (4), 3875−3886.
(38) Smith, M.; Gbur, G. Coherence resonances and band gaps in plasmonic hole arrays. *Phys. Rev. A* **2019**, *99*, 023812.
(39) Xiao, S.; Zhong, F.; Liu, H.; Zhu, S.; Li, J. Flexible coherent control of plasmonic spin-Hall effect. *Nat. Commun.* **2015**, *6*, 8360.
(40) Tetz, K. A.; Pang, L.; Fainman, Y. High-resolution surface plasmon resonance sensor based on linewidth-optimized nanohole array transmittance. *Opt. Lett.* **2006**, *31*, 1528−1530.
(41) Hajebifard, A.; Berini, P. Fano resonances in plasmonic heptamer nano-hole arrays. *Opt. Express* **2017**, *25*, 18566−18580.
(42) Wu, L.; Bai, P.; Zhou, X.; Li, E. P. Reflection and transmission modes in nanohole-array-based plasmonic sensors. *IEEE Photonics J.* **2012**, *4*, 26−33.
(43) Vala, M.; Ertsgaard, C. T.; Wittenberg, N. J.; Oh, S.-H. Plasmonic sensing on symmetric nanohole arrays supporting high-Q hybrid modes and reflection geometry. *ACS Sens.* **2019**, *4*, 3265−3274.

https://doi.org/10.1021/acsomega.1c07187
ACS Omega 2022, 7, 10420−10428